Molecular Crystals and Liquid Crystals

Publication details, including instructions for authors and subscription information:
http://www.tandfonline.com/loi/gmcl20

Molecular Modelling of the Morphology of Organic Crystals in the Presence of Impurity Species: Recent Applications to Naphthalene, Phenanthrene, and Caprolactam Crystals

G. Clydesdale [a], R. B. Hammond [a], V. Ramachandran [a], K. J. Roberts [a] & P. Mougin [b]

[a] Institute of Particle Science and Engineering, Department of Chemical Engineering, University of Leeds, Leeds, UK

[b] Institute of Particle Science and Engineering, Department of Chemical Engineering, University of Leeds, Leeds, UK and SSCI Inc., West Lafayette, Indiana, USA

Version of record first published: 31 Aug 2006

To cite this article: G. Clydesdale, R. B. Hammond, V. Ramachandran, K. J. Roberts & P. Mougin (2005): Molecular Modelling of the Morphology of Organic Crystals in the Presence of Impurity Species: Recent Applications to Naphthalene, Phenanthrene, and Caprolactam Crystals, Molecular Crystals and Liquid Crystals, 440:1, 235-257

To link to this article: http://dx.doi.org/10.1080/15421400590958566

Mol. Cryst. Liq. Cryst., Vol. 440, pp. 235–257, 2005

ISSN: 1542-1406 print/1563-5287 online
DOI: 10.1080/15421400590958566

Taylor & Francis
Taylor & Francis Group

Molecular Modelling of the Morphology of Organic Crystals in the Presence of Impurity Species: Recent Applications to Naphthalene, Phenanthrene, and Caprolactam Crystals

G. Clydesdale
R. B. Hammond
V. Ramachandran
K. J. Roberts
Institute of Particle Science and Engineering, Department of Chemical Engineering, University of Leeds, Leeds, UK

P. Mougin
Institute of Particle Science and Engineering, Department of Chemical Engineering, University of Leeds, Leeds, UK and SSCI Inc., West Lafayette, Indiana, USA

A molecular modelling capability for predicting the purity and morphology of solids manufactured via crystallisation is important in the realisation of a 'molecule-up' or product-centred, approach for the optimisation of chemical processes. Recent work on producing the morphology of molecular solids based upon the molecular and crystal chemistry is presented. The approach is based on the atom-atom method for calculating surface attachment energies, and from these relative crystal growth rates as a function of crystallographic growth direction. The computations have been recently [2,13–15] developed to be able to treat the effects of impurity species that influence morphology. Molecular modelling procedures include an optimisation of the position and orientation of the adsorbed additive within the host lattice hence, simulating the crystal chemistry of the hetero-species within the host lattice. Case studies include naphthalene and phenanthrene in the presence of biphenyl impurity and caprolactam in the presence of synthesis impurities.

Keywords: atom-atom method; biphenyl; caprolactam and α-glycine; habit modification; impurity incorporation; morphology; naphthalene; pheneanthrene; vacancy creation

Address correspondence to K. J. Roberts, Institute of Particle Science and Engineering, Department of Chemical Engineering, University of Leeds, Leeds LS2 9JT, UK. E-mail: k.j.roberts@leeds.ac.uk

1. INTRODUCTION

In the Chemical Industry, both in manufacturing and purification processes, separation of bulk and fine chemicals by crystallization plays a very important role. For example, control of particle shape and size during the manufacturing of chemicals such as agrochemicals, pharmaceuticals and dyestuffs can be manipulated giving the ability to predict and control crystal morphology [1–5]. Morphological modelling techniques have been based on the relation between crystal morphology and crystal lattice symmetry [6–8] and on the interaction energies between crystallizing units [9–11]. It is a well-known fact that the growth of crystals from solutions is strongly dependent both on the solvent employed and on the presence of heterospecies in the solution. Hence, it is important to see how the solvent and impurity molecules affect the growth rates of individual habit faces and hence modify the external morphology of the crystal.

Previous work has reviewed the use of the computer programme HABIT [4] to predict the crystal morphology of pure crystalline materials. The work has been extended to accommodate the effects of tailor-made impurities (molecules that resemble the host molecule) [12] on the predicted morphology of the pure crystals. In this, two categories of tailor-made additives were considered. The first of these is where the additive molecule is larger than the host molecule and hence blocks the growth of the layers [13,14] and the other where the additive is smaller or the same size as the host molecule and thus disrupts the growth of the layers [15]. In further studies, the work has been extended to enable an impurity molecule to be located at the position of the global minimum in calculated lattice energy within the host lattice [16] in order to achieve the best fit.

In this paper we present a review of the techniques used to model pure, solid organic materials and these materials in the presence of impurities or tailor-made additives. This is illustrated via a number of host/additive case studies including naphthalene/biphenyl, phenanthrene/biphenyl, and caprolactam/synthesis impurities systems. The basic methodology is explained in references [13–15] and some of the examples shown here (naphthalene/biphenyl, phenanthrene/biphenyl, caprolactam/synthesis impurities) have been detailed earlier [2] and [16].

2. CRYSTAL GROWTH THEORY AND ASSOCIATED MODELLING TECHNIQUES

2.1. Crystal Growth Models

A crystallisation process begins when a solution becomes supersaturated resulting in formation of nuclei in solution: the nucleation stage.

The solute clusters formed during nucleation remain in dynamic equilibrium due to the balance between the volume and surface contributions to their excess free energy. Once critical nucleus size is achieved the volume term dominates over the surface term and crystalline particles continue to grow. The relative rates of the nucleation and growth processes determine the size distribution of the emerging crystal phase. The nucleation stage is a 3-dimensional process in contrast to the crystal growth which is a 2-dimensional process where a stable cluster is developed by successive growth events taking place on structurally distinct growth faces. (see Fig. 1).

Perhaps the most elegant theoretical treatise is the pioneering work of Burton, Cabrera and Frank (BCF) [17] that has been the basis for the development of modern crystal growth theory. The BCF growth rate expression defines the relationship between the surface growth rate (R_{growth}) and the supersaturation (S) of the crystallising system as given below:

$$R_{growth} = AS^2 \tanh\left(\frac{B}{S}\right) \tag{1}$$

where, A and B are the temperature dependent constants. According to this and subsequent theories (volume diffusion model by Chernov [18], and simulation models [19,20]) crystal growth can be broadly classified into three major mechanistic regions which can be summarised as follow:

- at low supersaturations, the BCF equation reduces to $R_{growth} \propto S^2$ implying that growth at the crystal/liquid interface proceeds with a parabolic rate dependence.

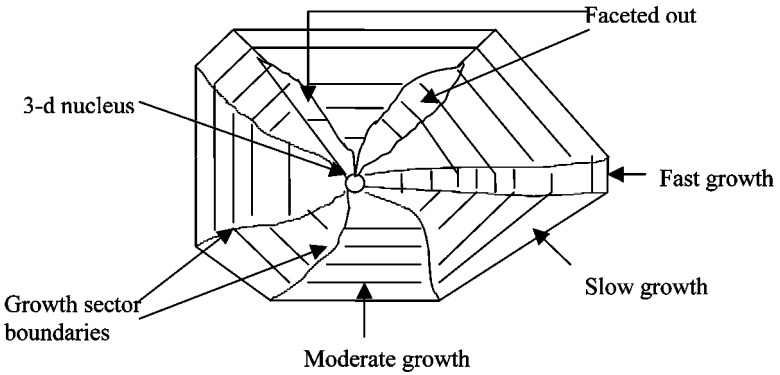

FIGURE 1 Schematic of the cut made through a 3-D crystal showing the simultaneous growth of the crystal along different interfaces.

- at moderate supersaturations surface integration can take place by 2-D surface nucleation via a birth and spread (B&S) mechanism [21] and Eq. (1) becomes $R_{growth} \propto S^{5/6} \exp(S)$.
- at high supersaturations, the law changes to $R_{growth} \propto S$. Here, interface (kinetic) roughening [22] takes place, meaning that the growth rate law changes from parabolic to linear. Here the growth interface is unstable and this is the rough interface growth (RIG) model.

Due to the different surface chemistry of the various crystal faces, each crystallographically unique face may grow by any one of the three interface kinetic processes. This variation in surface chemistry and hence surface binding with crystal orientation means that the growth and development of a crystal is likely to be anisotropic. In addition, depending on the relative growth rates of the crystal faces in three dimensions the particle morphology can be highly variable. Thus, the size and shape of a single particulate grain is governed both by the number of crystallographically independent faces and by the particular mechanisms by which a face grows.

The requirement for control of impurity levels in industrial crystallisation technology means that none of the crystal surfaces should grow under a RIG mechanism, to avoid resulting particles becoming excessively contaminated with impurities. The latter reflects the fact that molecular selectivity at the crystal growth interface can only operate effectively if crystallographic ordering is maintained.

2.2. Intermolecular Forces for Molecular Modelling

Discrete molecules which are the building blocks of crystals are held together by intermolecular forces. The dominant forces are the attractive van der Waals forces, repulsive forces due to the overlapping of the electron clouds, electrostatic interactions due to the partial charges on the atoms, and hydrogen-bonding. The sum of the intermolecular forces is a measure of the lattice energy or crystal energy (E_{cr}) and is expressed as

$$E_{cr} = \frac{1}{2}\sum_{k=1}^{N}\sum_{i=1}^{n}\sum_{j=1}^{n'} V_{kij} \tag{2}$$

This expression enshrines the atom-atom approach whereby the sum of the interaction energy of each atom with every other atom (of the adjoining molecules) is calculated. The terms have the following meanings:

n-number of atoms in the central molecule;
n'-number of atoms in each of the surrounding molecule

N-number of surrounding molecules
i-an atom on the central molecule
j-an atom in the surrounding *k*th molecule

V_{kij} - interaction energy between atom *i* in the central molecule and atom *j* in the nearby *k*th molecule. V_{kij} can be described by a number of intermolecular potential functions. Frequently used atom-atom potentials for molecular modelling are the Lennard-Jones (6–12) [23] and Buckingham [24] potentials given by :

$$V_{ij} = -\frac{A}{r_{ij}^6} + \frac{B}{r_{ij}^{12}} - \frac{q_i q_j}{r_{ij}} \tag{3}$$

and,

$$V_{ij} = -\frac{A}{r_{ij}^6} + B\exp(-Cr) - \frac{q_i q_j}{r_{ij}} \tag{4}$$

where A, B and C are empirical (atom specific) parameters. The terms q_i and q_j are the fractional charges on the *i*th and *j*th atoms respectively which are separated by a distance, r.

The validation of a selected intermolecular potential for a given system can be made by comparing the calculated lattice energy with the experimental lattice energy (V_{exp}), defined by:

$$V_{\exp} = -\Delta H_{sub} - 2RT \tag{5}$$

where ΔH_{sub} is the sublimation enthalpy with $2RT$ denoting the correction factor for the difference between the gas phase enthalpy and the vibrational contribution to the crystal enthalpy [25]. Table 1 gives the comparisons of calculated lattice energy and experimental lattice energy of some systems.

TABLE 1 Comparison of Some Calculated Lattice Energies with the Experimental Values from the Sublimation Enthalpy

	Lattice energy (kcal/mol)	
System	Calculated	Experimental
Glycine	−34.54 [41]	−33.69 [47]
L-alanine	−35.85 [46]	−34.09 [47]
Urea	−22.70 [25]	−22.20 [50]
Adipic acid	−33.8 [51]	−32.1 [25]
Benzoic Acid	−20.4 [51]	−23.0 [50]

2.3. Modelling Crystal Morphology in the Absence of Additives

The basis of morphological modelling techniques is correlating the external shape of the crystal and the internal crystal structure. In the Bravais-Friedel-Donnay-Harker (BFDH) approach [6–8] the most morphologically important forms (hkl) and hence those with the lowest growth rates are those having the greatest interplanar spacings d_{hkl}. However, the drawback of this approach is the neglect of the specific crystal chemistry of the material. It is relatively simple using this to predict morphologies which agree well with crystals observed experimentally in the case of molecular crystals without strongly directional bonding (e.g., hydrogen-bonding). However the approach is unable to correctly predict the morphology of crystal systems manifesting strongly anisotropic intermolecular forces. Hartman and Perdok [9,10] extended the ideas of the BFDH approach by including the intermolecular forces in the modelling process. This was achieved through the surface attachment energy (E_{att}) term which is defined as the energy released on the addition of a growth slice to the surface of a growing crystal [26] and is related to the crystallisation energy or lattice energy (E_{cr}) by:

$$E_{cr} = E_{sl} + E_{att} \tag{6}$$

E_{sl} is the slice energy or the intermolecular bonding energy contained within the surface growth slice (see Fig. 2). The growth rate of a given crystal face (hkl) is proportional to E_{att} and hence inversely to the morphological importance and E_{sl} [26]. The latter is thus a useful measure of the growth stability of a given crystal face. Both these energies are calculated by summing the potential energy that arises due to the intermolecular interactions between a molecule in the unit cell which is at the centre of the slice and all the molecules both inside and outside the slice of thickness d_{hkl}. For calculating the attachment energy, this process is repeated over all the molecules in the unit cell and then the value is averaged. By this approach the strength of individual intermolecular bonds can be evaluated. (Table 2 gives a sample list of intermolecular bonds listed according to their strength).

The position of the growth slice also needs to be optimized with respect to the slice energy. The slice energy optimization in the case of α-glycine is presented in Figure 3. In this it is noted that for the forms {020}, {110}, and {011} the optimum slice position is centred on the unit cell origin whereas for the {031} form it is centred at a distance $d_{hkl}/8$ from the unit cell origin. The growth morphology can be predicted using a classical Gibbs-Wulff polar plot [27,28] which is

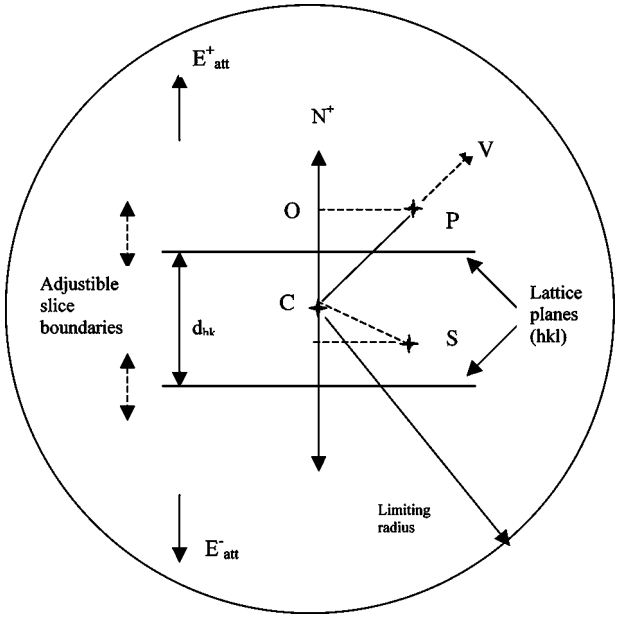

FIGURE 2 2-dimensional representation of the intermolecular interactions using atom-atom method in calculating attachment and slice energies within a sphere of limiting radius. C is the central molecule P is a molecule outside the slice, S is a molecule inside the slice, N^+ is the growth normal to the planes (hkl) and N^- is the growth normal to the planes (-h-k-l). d_{hkl} is the interplanar spacing, θ is the angle between the growth normal and the bonding vector CP. The slice boundaries are adjusted along the growth normal to maximize E_{slice} or the energetically most stable slice.

based on the assumption that E_{att} is directly proportional to the centre-to-face distance in a crystal as grown. Though this assumption of proportionality of the growth rate and E_{att} holds good for faces growing in layers, nevertheless we apply this for all faces and find a good correlation between observed and predicted morphologies [1,3–5, 14,15]. Some example morphologies as shown in Figure 4 demonstrate the ability of this methodology in predicting the shapes of a wide range of crystals [3].

Thus the main features of the methodology adopted for morphological prediction are,

- The initial molecular models are built using the molecular modelling programme, Cerius[2] [29] and then optimized using the semi-empirical methods using the programme MOPAC [30]. The crystallographically

TABLE 2 Intermolecular Bond Energies of α-Glycine (Attractive, Repulsive and Coulombic Energies are Given Separatedly) Listed According to their Strength. First z Stands for the Molecule in the Central Asymmetric Unit and the Second z Stands for the Molecule that is Displaced by uvw from the First z

						Energy (kcal/mol)			
Z	U	V	W	Z	DIST (Å)	ATT	REP	COUL	TOTAL
2	0	0	0	4	3.14	5.26	3.46	−5.31	−7.1
4	0	0	0	2	3.14	5.26	3.46	−5.31	−7.1
1	0	0	0	3	3.14	5.26	3.46	−5.31	−7.1
3	0	0	0	1	3.14	5.26	3.46	−5.31	−7.1
1	1	0	0	3	4.69	2.61	1.29	−5.24	−6.55
3	−1	0	0	1	4.69	2.61	1.29	−5.24	−6.55
2	−1	0	0	4	4.69	2.61	1.29	−5.24	−6.55
4	1	0	0	2	4.69	2.61	1.29	−5.24	−6.55

important forms are found via the BFDH method using the programme MORANG [31].

- The programme HABIT [8] is employed for the calculations of slice and attachment energies using the atom-atom method by the choice of a suitable potential.

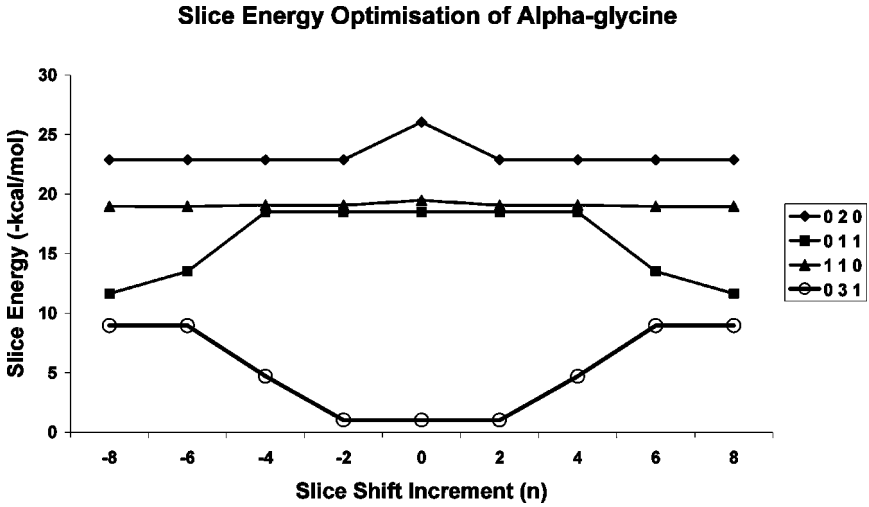

FIGURE 3 Optimisation of slice energy in the case of α-glycine. Slice shift increment is a multiple of d_{hkl} spacing.

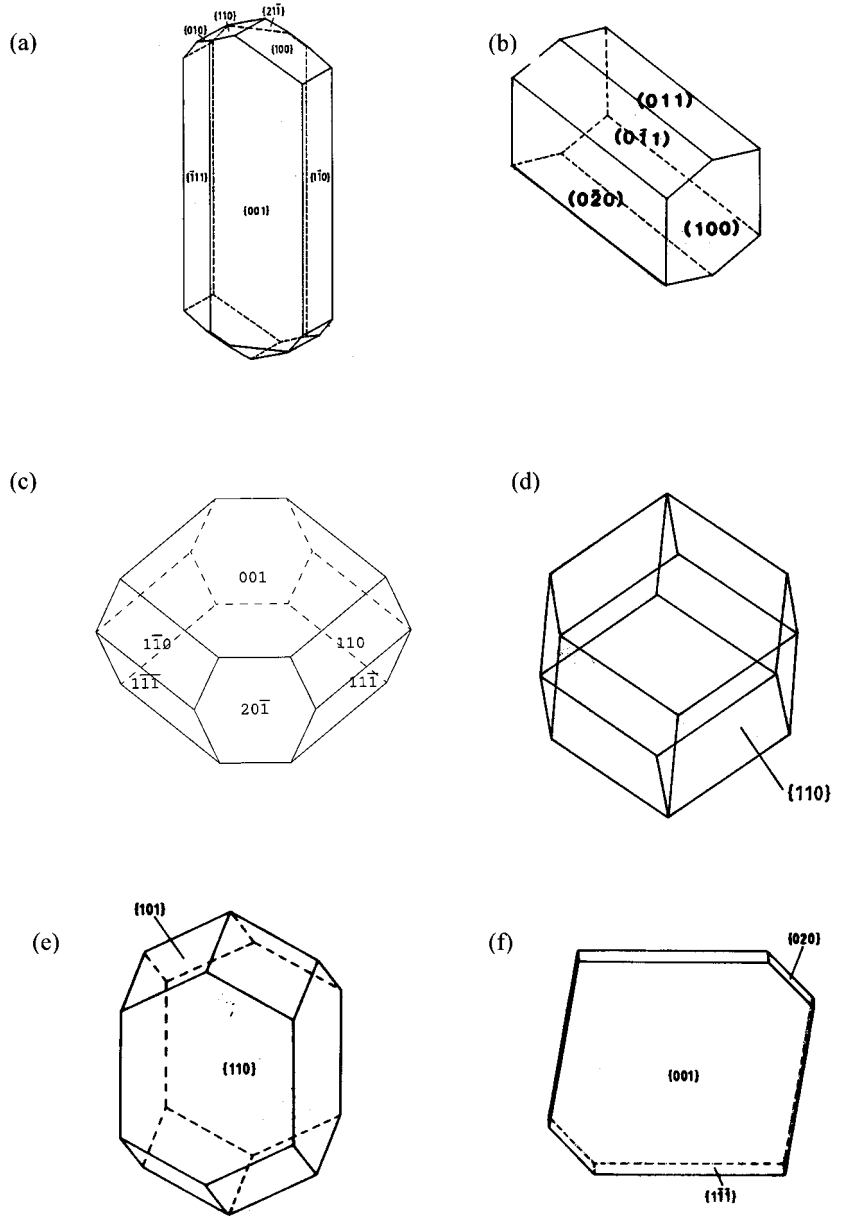

FIGURE 4 Some examples of predicted morphologies from [3]. (a) terephthalic acid, an aromatic acid, (b) nortriptyline hydrochloride, (c) naphthalene, (d) hexamine, (e) pentaerythritol tetranitrate, an organic explosive and (f) stearic acid, a long chain carboxylic acid.

- Once the attachment energies are calculated the morphology of the crystal is simulated using programmes like SHAPE [32] or CERIUS^2 [29].

2.4. Effect of Impurities or Tailor-made Additives on the Morphology of Crystals

Additives or impurities even in small amounts can affect the growth rates of the individual faces and in turn affect the morphology of the crystal itself. Once the impurity molecule gets into the crystal surface, it prevents host molecules from reaching the surface and thus changes the intermolecular bonding. In order to assess the likelihood of additive incorporation an additional factor is required which is the differential binding energy (Δb), the difference between the incorporation energies of pure host (E_H) and the additive (E_A) that is given by,

$$\Delta b = (E_A - E_H) = \left(E'_{sl} + E'_{ATT(+)} + E'_{ATT(-)}\right) - (E_{SL} + E_{ATT}) \qquad (7)$$

where E_{sl}' is the slice energy when the central molecule in the slice is an additive molecule and E'_{att} is the energy when a slice with an additive molecule is being incorporated to the growing pure host lattice (explained in Fig. 5). E'_{att} is the sum of $E'_{att(+)}$ and $E'_{att(-)}$. The two terms are considered separately as the additive can be incorporated either in the positive or in the negative growth direction. The additive incorporation takes place where Δb is at its minimum. If Δb is strongly dependant upon crystal orientation then the incorporation will be specific to one crystal face and vice versa.

Our methodology includes another parameter E''_{att} which is the energy released on the addition of a pure growth slice onto a surface on which an additive has adsorbed. This additional parameter can thus be used as a direct measure of the growth rate of a crystal face with an additive molecule present and hence the calculation of the crystal morphology modified due to the additive. The computer program HABIT [5,33] calculates the modified slice and attachment energies.

There are two modes for calculations evaluating the effect of an additive on a host crystal. In mode 1, one of the host molecules in the central unit cell within the slice is replaced by an additive molecule. Hence there will be $(Z - 1)$ host molecules in the central unit cell (where Z is the number of host molecules in a unit cell). When calculating the atom-atom interaction from the central additive molecule the values of $E'_{sl}(Z)$ and $E''_{att}(Z)$ [a sum of $E''_{att(+)}(Z)$ and $E_{att(-)}(Z)$] are obtained. These energies are averaged over all space-group symmetry related positions in one unit cell. In mode 2, an additive

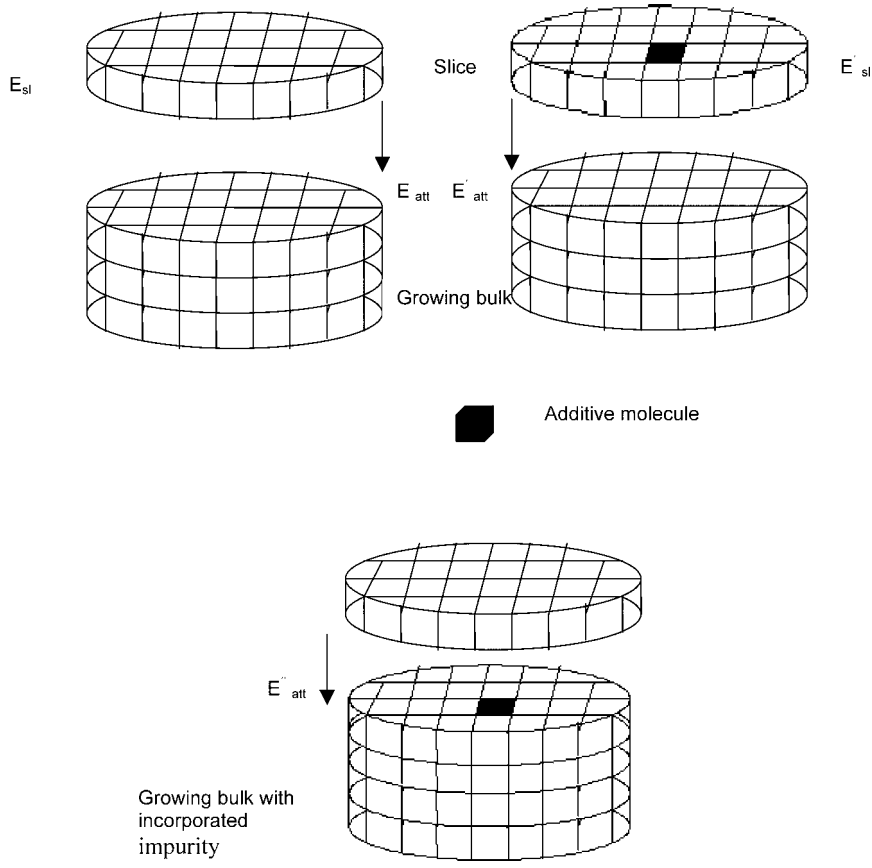

FIGURE 5 Schematic representing E_{sl} (slice energy of pure host molecules), E'_{sl} (slice energy with an impurity molecule incorporated into it), Eatt (attachment energy when a pure host slice is adsorbed onto a growing bulk of pure host molecules), E'_{att} (attachment energy when a slice containing an incorporated additive molecule is adsorbed onto a growing bulk of pure host molecules) and E''_{att} (Attachment energy when a pure host slice is being adsorbed by a growing bulk with an impurity molecule on the top layer).

molecule replaces the nearest molecule outside the slice. The central unit cell contains solely the host molecules. In this mode $E_{sl}(Z)$ and $E'_{att(+)}(Z)$ and $E'_{att(-)}(Z)$ are calculated by the program. The differential binding energy is calculated as given in Eq. 9 which can be rewritten as:

$$\Delta b = E'_{sl} - E_{sl} - \Delta E^{UVWZ}_{att} \tag{8}$$

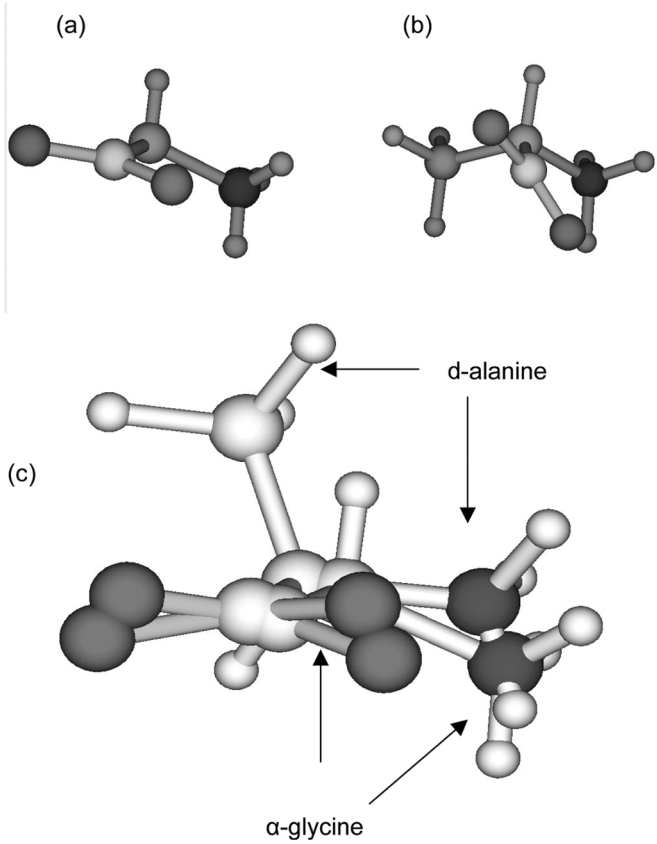

FIGURE 6 Molecular structures of (a) α-glycine and (b) d-alanine In these two molecules the hydrogen from the carboxylic group (COOH) is attracted to the amino group (NH_2) and it becomes NH_3. (c) The fitted and optimised d-alanine molecule onto an α-glycine molecule within INTERCHEM (red sphere denotes oxygen, blue sphere denotes nitrogen, large grey denotes carbon and small grey sphere denotes hydrogen atoms).

where ΔE_{att}^{UVWZ} is the difference in molecule-molecule interaction energy between a host molecule in the central unit cell within the slice and the closest host molecule outside the slice, E_{att} (referenced by the unit cell directions U,V,W and the symmetry position, Z), and the interaction energy between a host molecule in the central unit cell and an additive molecule which replaces the closest host molecule outside the slice, E'_{att}.

The fitting of an additive molecule on to a host lattice is achieved by superimposing a single additive molecule on a single host molecule

within the modeling package INTERCHEM [34] using the common moieties of both molecules (see for example Fig. 6 of α-glycine and l-alanine). This method minimizes the rms difference of the Cartesian coordinates of the corresponding atoms and converts the additive atom positions to fractional coordinates in terms of the host lattice. The additive molecule then substitutes the host molecule, which is used to locate the additive, for the purposes of the optimization procedure.

For a given additive molecule values of Δb less than 10 kcal/mol are considered sufficiently low to allow impurity incorporation on these faces, and E''_{att} defines the growth rates. When Δb is large, an additive cannot be incorporated on that particular face and host E_{att} values decide the growth rates. In this procedure all of the asymmetric units of the host system within a unit cell are considered in turn and this allows a predictive calculation of the impurity-modified crystal morphology.

2.5. Global Optimization of Additive within Host Lattice

Optimizing the orientation of the additive allows the calculation of a more physically realistic value for the differential binding energy (Δb). In order to achieve optimization of the impurity molecules within the host crystal lattice environment, minimization of the calculated lattice energy is employed. In this, the position and orientation of the impurity molecule are as a rigid body allowed to vary whereas the position and orientation of the host molecules are kept fixed.

As a front-end to the above procedure, the centre of gravity coordinates of the impurity molecule as defined via the fitting procedure are used to define a centre of rotation. Rotation angles with respect to the three Cartesian axes in the following ranges: $-180^\circ \leq \theta_x < 180^\circ$, $-180^\circ \leq \theta_y < 180^\circ$, $0^\circ \leq \theta_z < 180^\circ$ and a step size of 60° were employed. The approach defines a coarse, three dimensional grid with 108 points in the rotational space of the impurity molecule (treated as a rigid body) hence providing an un-biased matrix of starting structures for subsequent minimization.

To locate each point on the grid, the requisite rotations are applied to the atomic Cartesian coordinates of the additive molecule as derived from the r.m.s. fitting routine. Lattice energy minimisation is then carried out starting from each location on the grid. The calculated lattice energies are then ranked from the lowest (most stable) to the highest (least stable). After ranking the minima, if the same minimum is located more than once, the lowest lattice energy obtained is taken to indicate the global optimum-position. Thus by this grid search

approach, a global minimum instead of a local minimum is achieved, in principle, without any ambiguity.

It is important to note, however, that the above methodology does not account for any local perturbation of the host lattice due to the incorporation of additive molecules in the crystal. This could be one of the future developments to be considered in the methodology. In addition, in this methodology the energy optimization is carried out within the bulk host crystal lattice rather than at specific crystal surfaces.

The vacancy creation procedure follows the grid optimisation stage. The best optimised position (out of the 108 starting positions) is selected from which the preferred orientation of the additive is extracted and a molecule-molecule energy breakdown of the lattice energy is recorded. From this energy breakdown the host molecules that are least energetically compatible with the impurity molecule in its optimum position are identified. These particular host molecules are omitted to create vacancies. The additive molecule is optimized for a second time with the same starting position but with vacancies in the host lattice. As an example, the optimised fit of a d-alanine molecule on a α-glycine molecule is shown in Figure 6. Following this procedure, attachment energies are calculated in blocker mode of the programme HABIT [4].

3. SOME EXAMPLES OF PREDICTED MORPHOLOGIES

3.1. Effects of Biphenyl on the Morphology of Naphthalene and Phenanthrene.

Naphthalene is an aromatic hydrocarbon with two fused benzene rings. It crystallizes in the monoclinic space group $P2_1/a$ in a bimolecular unit cell of dimensions $a = 8.098$ Å, $b = 5.953$ Å, $c = 8.652$ Å and $ß = 124.4^\circ$ [35]. Biphenyl also crystallizes in bimolecular unit cell in the space group $P2_1/a$ with dimensions $a = 8.120$ Å, $b = 5.630$ Å, and $c = 9.510$ Å with $ß = 95.10^\circ$ [36]. The crystallographic data were taken from reference [35]. The intermolecular interactions for both naphthalene and phenanthrene were calculated using a combined Buckingham/Coulombic potential [25]. The calculated lattice energies of naphthalene and phenanthrene are -19.4 kcal/mol and -24.60 kcal/mol respectively. The attachment energies and from these the relative rates of growth of the most prominent faces were calculated. The differential binding energies and attachment energies of naphthalene (both pure and biphenyl incorporated) are presented in Table 3. These results are taken from [2]. From this table it is

TABLE 3 Differential Binding Energy and Attachment Energies (kcal/mol) of Pure Naphthalene, Phenanthrene, Naphthalene with Biphenyl and Phenanthrene with Biphenyl [2]

Relaxed biphenyl naphthalene				Relaxed biphenyl in phenanthrene			
(hkl)	Δb	E''_{att}	E_{att}	(hkl)	Δb	E''_{att}	E_{att}
001	433.98	−6.18	−5.97	001	3.14	−5.37	−5.79
11 − 1	1.06	−9.20	−12.24	100	1.72	–6.87	−8.74
110	0.67	−8.30	−11.77	10–1	1.49	−9.14	−11.23
20 − 1	12.58	−10.97	−13.08	0–11	2.48	−14.78	−16.75

noted that due to the high value of Δb, the (001) face is not affected by the impurity, biphenyl. Thus the morphology of the host crystals were predicted as shown in Figures 7 and 8.

The effects of the presence of biphenyl as an impurity on the morphologies of naphthalene and phenanthrene were examined. In the case of naphthalene crystals, the relaxed biphenyl impurity finds (110) faces are the most favourable faces for incorporation (low Δb values) while the unrelaxed additive biphenyl suggests that (11−1) is the best site for impurity incorporation Figure 7 shows that (110) is the most favourable face for biphenyl incorporation. Note that fewer vacancies are required when the additive is allowed to relax its orientation, in other words, creation of a larger number of vacancies than necessary results in a physically unrealistic loss of energy or lowering of E''_{att}.

The differential binding energy and attachment energies of phenanthrene (both pure and biphenyl on phenanthrene) are shown in Table 3 [2]. The morphology of a phenanthrene crystal influenced by biphenyl is shown in Figure 8. It is observed the face (001) decreases in importance with lower E''_{att} while the face (10−1) increases in importance.

3.2. Morphology of Pure Caprolactam and Its Modifications Due to Synthesis Impurities.

In one of the routes in the commercial process of crystallisation of ε-caprolactam, various side-products, as cyclohexane, cyclohexanol and cyclohexanone are formed. Due to their similarity to caprolactam in terms of molecular structure, these intermediates are known to affect the crystallisation of the final caprolactam. However, the incorporation of the tautomeric form “impurity” Caprolactim, into the host

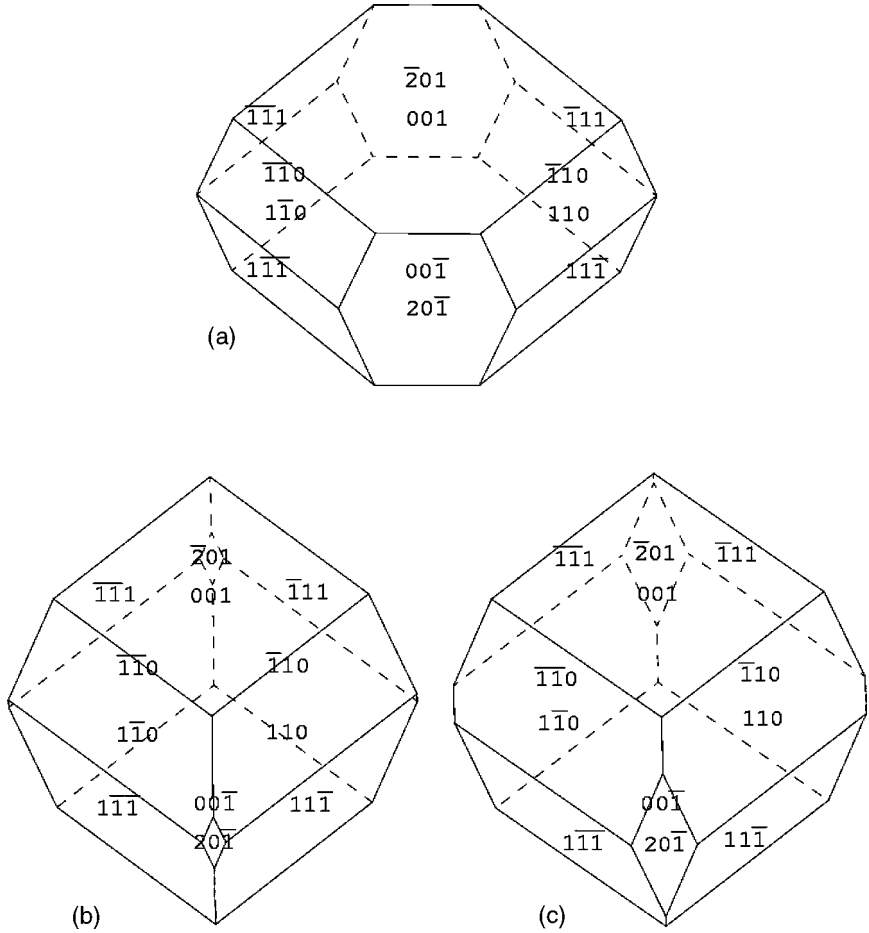

FIGURE 7 Predicted morphology of (a) pure Naphthalene, (b) effect of unrelaxed biphenyl on the predicted morphology of naphthalene, and (c) effect of relaxed biphenyl on naphthalene.

ε-caprolactam lattice is not straightforward as it is not tailored to the host molecule.

ε-caprolactam crystallises in space group C2/c, [37] with a monoclinic unit cell: $a = 19.28$ Å, $b = 7.78$ Å, $c = 9.57$ Å and $\beta = 112.39^{\circ}$ with eight molecules in the unit cell. The potential parameters given by Momany et al [38] were used for the calculation. The calculated lattice energy of the host ε-caprolactam is -16.5 kcal/mol. This compares satisfactorily with the value of the sublimation enthalpy (20.6 kcal/mol at 338 K [39] and 20.8 kcal/mol at 342 K [40]).

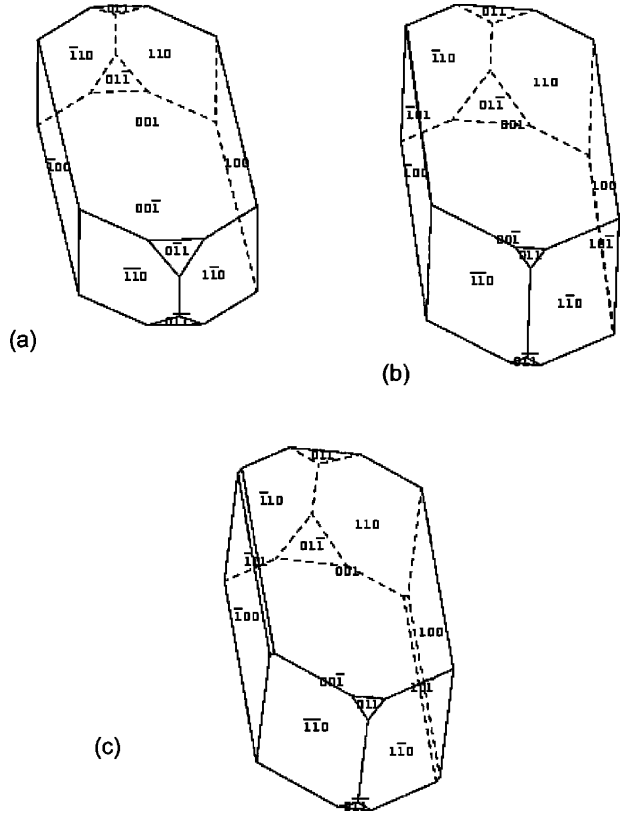

FIGURE 8 Predicted morphology of (a) pure phenanthrene, (b) effect of unrelaxed biphenyl on the morphology of phenanthrene and (c) effect of relaxed biphenyl on phenanthrene.

The optimum positions of the additive molecules, cyclohexanol, cyclohexanone and caprolactim in the host lattice are shown in Figure 9. See below the figure for explanations regarding the interatomic bonds.

The calculated differential binding energies, attachment energies and relative growth rates of cyclohexane and cyclohexanol on the crystallographically most important faces of ε-caprolactam are given in Table 4. The values shown here are for the optimized positions of the additive in the host lattice. From this table it is noted that *cyclohexane* is unlikely to partition into the three most important forms to any great extent due to the high values of the differential binding energies. The forms $\{31\ -1\}$, $\{111\}$, $\{20\ -2\}$ and $\{40\ -2\}$ of ε-caprolactam

TABLE 4 Differential Binding Energies, Attachment Energies and Relative Growth Rates of Cyclohexane (1) and Cyclohexanol (2) in the Pure Host ε-Caprolactom

Growth face	Differentail binding energy optimised Δb (kcal/mol)		Optimised AE for host onto impurity containing slice E''_{att} (kcal/mol)		AE for host on pure host slice E_{att} kcal/mol	Relative growth rates scaled on optimised AE of (200) face		
	Cyclohexane 1	Cyclohexanol 2	Cyclohexane 1	Cyclohexanol 2		1	2	Host
(200)	6.31	3.45	−3.71	−3.75	−4.01	1.00	1.00	1.00
(110)	5.20	2.26	−3.98	−3.98	−5.33	1.07	1.06	1.33
(11 − 1)	4.81	3.30	−4.94	−6.36	−6.68	1.33	1.70	1.67
(111)	3.33	1.86	−6.07	−7.54	−9.30	1.64	2.01	2.32
(31 − 1)	4.15	2.79	−5.48	−7.06	−7.88	1.48	1.88	1.97
(20 − 2)	2.33	2.25	−6.82	−9.36	−11.21	1.84	2.57	2.80
(310)	3.12	1.62	−6.24	−7.67	−9.67	1.68	2.05	2.41
(002)	2.16	2.00	−6.90	−9.64	−11.46	1.86	2.57	2.86
(11 − 2)	1.25	0.58	−6.89	−9.16	−12.19	1.86	2.44	3.04
(40 − 2)	2.67	2.69	−7.02	−9.93	−11.07	1.89	2.65	2.76

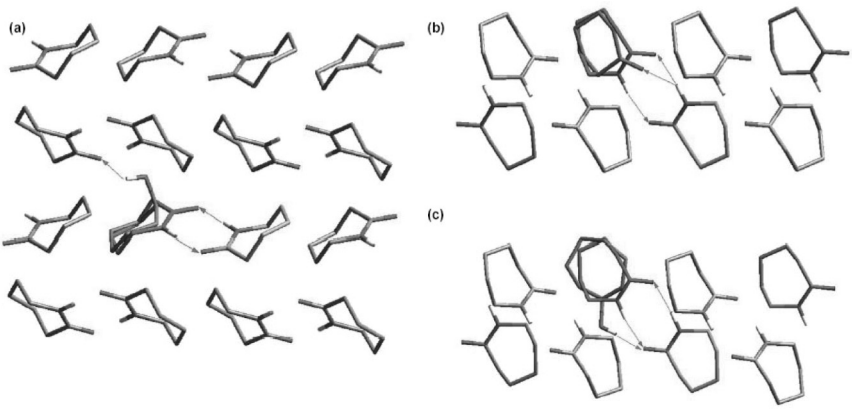

FIGURE 9 Optimal position of the impurity molecules (a) cyclohexanol, (b) cyclohexanone and (c) caprolactim in the ε-caprolactam host. Carbon atoms of the impurity molecule coloured green, of the substituted caprolactam molecule magenta and of the caprolactam molecule for which the hydrogen-bonded interactions are missing orange. The hydrogen bonds that are broken on substitution of an impurity molecule for a host molecule are indicated by red arrows that formed by a green arrow.

are the most affected due to the impurity cyclohexane. The modified morphology of ε-caprolactam with cyclohexane is shown in Figure 10.

It is observed from Table 4 that for *cyclohexanol* of the three predominant faces the most likely face into which the impurity incorporation takes place is (110). In addition, the forms {111}, {31 – 1}, and {20-2} also appear in the morphology of the caprolactam crystal which contains cyclohexanol impurity (Fig. 10).

The differential binding energies, attachment energies and the relative growth rates of cyclohexanone and caprolactim are given in Table 5. In the case of cyclohexanone it is noted from the table that the differential binding energies for the forms {200}, {110} and {11 – 1} are similar. From Figure 10, it is observed that there is not much difference between the predicted morphology of the pure host and that when the impurity cyclohexanone is present, except for the presence of a significant {002} form and the appearance of the {20 – 2} form.

The effect due to the presence of the imino tautomeric form of caprolactam on the morphology of ε-caprolactam is shown in Figure 10. The differential binding energies for the three prominent forms are small. Hence the impact of caprolactim on the reduction of growth rates on all the faces of caprolactam will be similar.

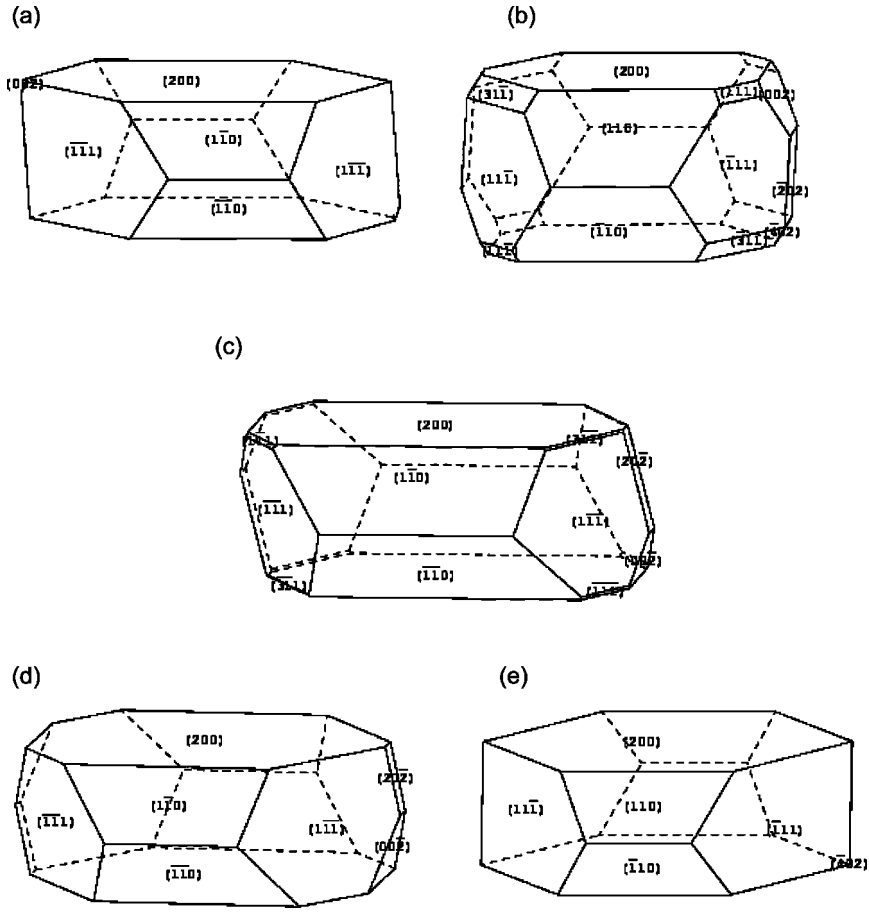

FIGURE 10 Calculated morphologies for (a) pure ε-caprolactam and ε-caprolactam in the presence of (b) cyclohexane, (c) cyclohexanol, (d) cyclohexanone, (e) caprolactim.

6. CONCLUSIONS

In this paper the basic approach to predicting crystal morphology based on intermolecular (non-bonded) interaction energies, drawing down on the crystallographic structures of the materials, is presented with particular emphasis on impurity effect processes. In our approach the additive molecules were fitted and relaxed within the host lattice which was treated as rigid. One of the future developments to this approach is to see how the crystal shape will be affected by relaxing the host lattice around the site of the impurity.

REFERENCES

[1] Docherty, R. & Roberts, K. J. (1988). Modelling the morphology of molecular crystals; application to anthracene, biphenyl and ß-succinic acid. *J. Cryst. Growth*, *88*, 159 –168.

[2] Clydesdale, G., Hammond, R. B., & Roberts, K. J. (2003). Molecular modeling of bulk impurity segregation and impurity-mediated crystal habit modification of naphthalene in the presence of heteroimpurity species. *J. Phys. Chem. B*, *107*, 4826–4833.

[3] Clydesdale, G., Roberts, K. J., & Walker, E. M. (1997). The crystal habit of molecular materials: A structural perspective. In: *Theoretical Aspects and Computer Modelling.* Gavezzotti, A. (Ed.), John Wiley & Sons Ltd: Chichester, 203–232.

[4] Clydesdale, G., Roberts, K. J., & Docherty, R. (1991). HABIT–A programme for predicting the morphology of molecular crystals. *Comp. Phys. Comm.*, *64*, 311–328.

[5] Clydesdale, G., Roberts, K. J., & Docherty, R. (1996). HABIT95–A program for predicting the morphology of molecular crystals as a function of the growth environment. *J. Cryst. Growth*, *166*, 78–83.

[6] Bravais, A. (1866). *Etudes Crystallographiques*, Gauthier-Villars: Paris.

[7] Friedel, G. (1907). *Bull. Soc. Franc. Mineral*, *30*, 326.

[8] Donnay, J. D. H. & Harker, D. (1937). *Am. Mineralogist*, *22*, 446.

[9] Hartman, P. & Perdock, W. G. (1955). *Acta Cryst.*, *8*, 49.

[10] Hartman, P. & Perdock, W. G. (1955). *Acta Cryst.*, *8*, 521.

[11] Berkovitch-Yellin, Z. (1985). Toward an ab initio derivation of crystal morphology. *J. Am. Chem. Soc.*, *107*, 8239–8253.

[12] Lahav, M., Leiserowitz, Z., Berkovitch-Yellin, J., van Mil, Addadi, L., & Idelson, M. (1985). Crystal morphology engineering by tailor-made inhibitors; A new probe to fine intermolecular interactions. *J. Amer. Chem. Soc.*, *107*, 3111–3122.

[13] Clydesdale, G., Roberts, K. J., & Lewtas, K. (1994). *Mol. Cryst. Liq. Cryst.*, *248*, 243–276.

[14] Clydesdale, G., Roberts, K. J., Lewtas, K., & Docherty, R. (1994). Modelling the morphology of molecular crystals in the presence of blocking tailor-made additives. *J. Cryst. Growth*, *141*, 443–450.

[15] Clydesdale, G., Roberts, K. J., & Docherty, R. (1994). Modelling the morphology of molecular crystals in the presence of disruptive tailor-made additives. *J. Cryst. Growth*, *135*, 331–340.

[16] Mougin, P., Clydesdale, G., Hammond, R. B., & Roberts, K. J. (2003). Molecular and solid-state modeling of the crystal purity and morphology of ε-caprolactam in the presence of synthesis impurities and the imino-tautomeric species Caprolactim. *J. Phys. Chem. B*, *107*, 13262–13272.

[17] Burton, W. K., Cabrera, N., & Frank, F. C. (1951). *Phil. Trans. Roy. Soc.*, *243*, 299.

[18] Chernov, A. A. (1961). The spiral growth of crystals. *Soviet Physics Uspechi*, *4*, 116–118.

[19] O'Hara, M. & Reid, R. C. (1973). *Modelling Crystal Growth Rates from Solution*. Prentice-Hall: Englewood Cliffs.

[20] Bennema, P. & Van der Eerden, J. P. (1987). Chapter 1. In: *Morphology of Crystals*, Sunagawa, I. (Ed.), Terra Scientific Publishing Company: Tokyo.

[21] Gilmer, G. H. & Jackson, K. A. (1977). In: *Crystal Growth and Materials*, Kaldis, E. & Scheel, H. J. (Eds.), Amsterdam, 80–114.

[22] Jackson, K. A. (1958). *Liquid Metals and Solidification*, American Society for Metals: Cleveland, Ohio.

[23] Lennard-Jones, J. E. (1924). *Proc. Roy. Soc.*, *A106*, 442.

[24] Buckingham, R. A. & Corner, J. (1947). *Proc. Roy. Soc*., *189*, 118.
[25] Williams, D. E. (1966). Nonbonded Potential Parameters derived from crystalline aromatic hydrocarbons. *J.Chem. Phys*., *45*, 3770–3778.
[26] Bennema, P. & Hartman, P. (1980). The attachment energy as a habit controlling factor. *J. Cryst. Growth*, *49*, 145–156.
[27] Gibbs, J. W. Trans. Acad. Connecticut Acad. 1875; 3. also The equilibrium of Heterogeneous substances. Scientific papers. 1906; 1. and Collected Works. New York: 1928.
[28] Wulff, G., *Z. Krist*. (1901). *34*, 499.
[29] CERIUS^2 Molecular Modelling Software for Materials Research by Accelrys Inc., Princeton NJ. 2000.
[30] MOPAC, version 6.0: Quantum Chemistry Program Exchange Program No. 455. Creative Arts Building 181, Indiana University, Bloomington, IN 47405.
[31] Docherty, R., Roberts, K. J., & Dowty, E. (1988). MORANG–A computer program designed to aid in the determinations of crystal morphology. *Computer Physics Communications*, *51*, 423–430.
[32] Dowty, E. (1980). Computing and drawing crystal shapes. *Am. Mineralogist*, *65*, 465–471.
[33] Clydesdale, G., Roberts, K. J., & Docherty, R. J. (1996). *Quantum Chemsitry Program Exchange*, *16*, 1.
[34] Bladon P: Interchem-PC software Version 3.4, http://www.interprobe.co.uk/inter/interprobe.html. 2002.
[35] McArdle, B. J. & Sherwood, J. (1985). *N. Chem. Ind*., April 269.
[36] Trotter, J. (1961). The crystal and molecular structure of biphenyl. *Acta Cryst*., *14*, 1135–114.
[37] Winkler, F. K. & Dunitz, J. D. (1975). Structural crystallography and crystal chemistry. *Acta Cryst. B*, *31* 268–269.
[38] Momany, F. A., Carruthers, L. M., Mcguire, R. F., & Scheraga, H. A. (1974). Interemolcular potentials from crystal data. III. Determination of empirical potentials and application to the packing configurations and lattice energies in crystals of hydrocarbons, carboxylic acids, amines and amides. *J. Phys. Chem*., *78*, 1595–1620.
[39] Kabo, G. T., Kozyro, A. A., Krouk, V. S., Sevruk, V. M., Yursha, I. A., Simirsky, V. V., & Gogolinsky, V. I. (1992). *J. Chem. Thermodyn*., *24*, 1–13.
[40] Steele, W. V., Chirico, R. D., Knipmeyer, S. E., & Nguyen, A. (2002). Measurements of vapour pressure, heat capacity and density along the saturation line for ε-caprolactam, Pyrazine, 1,2 Propanediol, Triethylene glycol, Phenyl acetylene and Diphenyl acetylene. *J. Chem. Eng. Data*, *47*, 689–699.
[41] Johnsson, P. G. & Kvick, A. (1972). Precision neutron diffraction structure determination of protein and nuclei acid componenets. III. The crystal and molecular structure of the amino acid α-glycine. *Acta Cryst B*, *28*, 1827–1833.
[42] Perlovich, G. L, Hansen, L. K., & Bauer-Brand, A. (2001). The polymerism of glycine. *J. Thermal Analysis and Calorimetry*., *66*, 699–715
[43] Weissbuch, I., Addadi, L., Berkovitch-Yellin, Z., Gati, E., Weinstein, S., Lahav, M., & Leiserowitz, L. (1983). Centrosymmetric crystals for the direct assignment of the Absolute configuration of chiral molecules. Application to the α-amino acids by their effect on glycine crystals. *J. Am. Chem. Soc.*, *105*, 6615–6621.
[44] Iitaka, Y. (1961). The crystal structure of γ-glycine. *Acta Cryst.*, *14*, 1–8.
[45] Marsh, R. E., (1958). A refinement of the crystal structure of glycine. *Acta Cryst.*, *11*, 654–663.
[46] Destro, R., Marsh, R. E., Bianchi, R. (1988). A low temperature study of l-alanine. *J. Phys. Chem.*, *92*, 966–973.

[47] Svec, H. J. & Clyde, D. D. (1965). Vapour pressures of some α-amino acids. *J. Chem. Eng. Data.*, *10*, 151–152.
[48] Lin, C. H., Gabas, N., Canselier, J. P., Pepe, G. (1998). Prediction of growth morphology of aminoacid crystals in solution I. α-glycine. *J. Cryst. Growth*, *191*, 791–802.
[49] Bisker-Leib, V. & Docherty, M. F. (2003). Modelling crystal shape of polar organic materials: Applications to amino acids. *Cryst. Growth and Design*, *3*, 221–237.
[50] Cox, J. D. & Pilcher, G. (1959). *Thermochemistry of Organic and Organometallic Compounds*. Academic Press: New York, B2, 1242.
[51] Lifson, S., Hagler, A. T., & Dauber, P. J. (1979). *American Chem. Soc.*, *101*, 5111.